New Magnetically Coupled Bimetallic Complexes as Potential Building Blocks for Magnetic Materials

Scott W. Gordon-Wylie, Brian L. Claus, Colin P. Horwitz, Yan Leychkis, José M. Workman, Alexander J. Marzec, George R. Clark, Clifford E. F. Rickard, Brenda J. Conklin, Scott Sellers, Gordon T. Yee, and Terrence J. Collins*

Abstract: The preparation and characterization of the new binucleating ligand, 1,2,4,5-tetrakis(2-hydroxy-2-methylpropanamido)benzene, H_8[**3**], and its Co^{III} and $V^{V}(O)$ complexes $[PPh_4]_2$[$Co^{III}(\kappa^4$-**3**-$\kappa^4)Co^{III}$], $[PPh_4]_2$[**4**], and $[Et_4N]_2[V^{V}(O)(\kappa^4$-**3**-$\kappa^4)V^{V}(O)]$, $[Et_4N]_2$-[**5**], are described. Both complexes have been characterized by X-ray crystallography, ^{1}H NMR, IR, and UV/Vis spectroscopy, and by electrochemical and microanalytical analyses. The electrochemical properties of $[\mathbf{4}]^{2-}$ and $[\mathbf{5}]^{2-}$ are remarkably similar, each exhibiting two one-electron oxidation processes of similar $E^{\circ\prime}$; since the $V^{V}(O)$ sites in $[\mathbf{5}]^{2-}$ are d^0, ligand-localized oxidation is implicated for both compounds. A deep blue vanadium species obtained upon one-electron oxidation of $[\mathbf{5}]^{2-}$, $[\mathbf{5^I}]^{-}$, has a total spin, S_T, of 1/2, and its EPR spectrum exhibits a single $g = 2$ signal at 4 K. These results are consistent with the oxidized vanadium complex, $[\mathbf{5^I}]^{-}$, as containing the ligand cation radical **3^I**, that is $[\mathbf{5^I}]^{-}$ is best formulated as $[V^{V}(O)(\kappa^4$-**3^I**-$\kappa^4)V^{V}(O)]^{-}$. Isolation and characterization of the dark purple cobalt species, obtained upon one-electron oxidation of $[\mathbf{4}]^{2-}$, $[\mathbf{4^I}]^{-}$, also revealed the presence of the organic radical **3^I**. Magnetic susceptibility data for $[\mathbf{4}]^{2-}$ revealed that exchange coupling (the Hamiltonian convention $+J\,S_i \cdot S_j$ is used throughout) between the two axial $S = 1$ Co^{III} centers was very weak (that is $J_{Co^{III}-Co^{III}} \approx 0\ cm^{-1}$). In contrast, for $[\mathbf{4^I}]^{-}$, the ground spin state of $S_T = 3/2$ and the observed EPR spectrum and magnetic susceptibility data can be rationalized by the relatively strong antiferromagnetic coupling between each rhombic $S = 1$ Co^{III} ion and an $S = 1/2$ ligand cation radical ($J_{Co^{III}-\mathbf{3}^I} \approx 75\ cm^{-1}$). Such a ferrimagnetic system serves to align the Co^{III} spin centers in a common direction, an important step towards building ferromagnetic or ferrimagnetic network solids.

Keywords: cobalt · EPR spectroscopy · magnetic properties · radical ions · vanadium

Introduction

The design of magnetic materials with building blocks comprising multimetallic coordination compounds is attracting attention, fueled in part by the assumption that useful magnetic materials can be obtained.[1–7] Theoretical treatments have provided design principles, linking features of the molecular and electronic structures so that the sign and/or magnitude of the exchange interactions can be predicted.[7–9] Recently, we proposed a design principle,[10, 11] in which the electronic structure of one magnetic ion, M_a, of an interacting pair, $M_a - M_b$, can be shaped by strong ligand σ-donor properties; this control of the electronic structure at M_a allows one to predict the sign of the exchange interactions with any M_b ion. For the Co^{III} complex $[\mathbf{1}]^{-}$ (Scheme 1), the unusual $S = 1$ electronic configuration is generated by the influence of the diamido-*N*-dialkoxido ligand system. This complex serves as the M_a unit in the multinuclear D_3 ion, $[\mathbf{2}]^{-}$ (Scheme 1), in which Co^{II} is the M_b ion. From the unusual orbital configuration at Co^{III}, local control[10, 11] can be attained over the sign of the $Co^{III} - Co^{II}$ exchange interaction in $[\mathbf{2}]^{-}$, wherein Co^{III} and Co^{II} are ferromagnetically coupled (the Hamiltonian convention used was $+J\,S_i \cdot S_j$) with $J_{Co^{III}-Co^{II}} \approx -25\ cm^{-1}$.[10, 11]

In order to extend the presumed local control of magnetic coupling occurring in $[\mathbf{2}]^{-}$ to expanded arrays of multimetallic ions, we set out to synthesize a dimeric analogue of $[\mathbf{1}^{-}]$. The binucleating ligand system $[\mathbf{3}]^{8-}$ preserves the strongly σ-

[*] Prof. T. J. Collins, S. W. Gordon-Wylie, B. L. Claus, C. P. Horwitz
Y. Leychkis, J. M. Workman, A. J. Marzec
Department of Chemistry, Carnegie Mellon University
4400 Fifth Avenue, Pittsburgh, Pennsylvania 15213 (USA)
Fax: (+1) 412 268-1061
E-mail: tc1u@andrew.cmu.edu
Prof. G. T. Yee, S. Sellers, B. J. Conklin
Department of Chemistry and Biochemistry
University of Colorado at Boulder
Campus Box 215, Boulder, Colorado 80309 (USA)
Prof. G. R. Clark, Prof. C. E. Rickard
Department of Chemistry, University of Auckland
Private Bag 92019, 23 Symonds Street, Auckland (New Zealand)

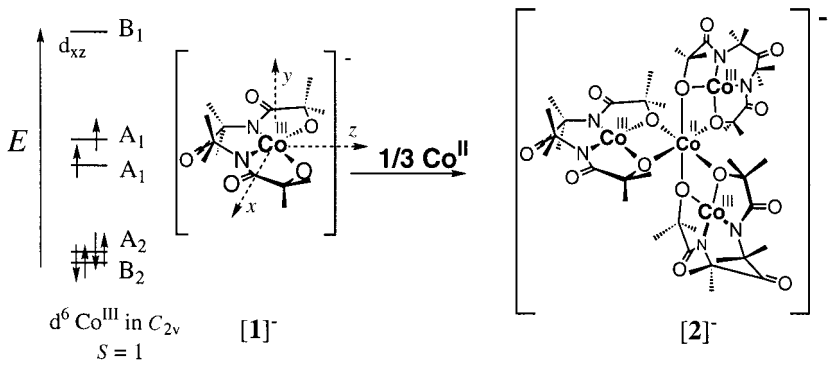

Scheme 1.

donating ligand framework found in $[\mathbf{1}]^-$, holds in a planar array two primary magnetic ions, M_a, and has the potential to link additional magnetic ions, M_b, in extended arrays. For example, bimetallic M_a complexes of $[\mathbf{3}]^{8-}$ would appear to be candidates for forming linear arrays based upon tetrahedral or planar four-coordinate M_b ions, or hexagonal sheets, or helical structures based upon D_3 M_b ions.[10] If high T_c magnetic materials are to be obtained, a magnetic pathway must be present to link all the component M_a metal ions. Moreover, if such an approach is to successfully yield a crystalline material, it is important that the binding of the secondary ions, M_b, is weak enough under the formation conditions to allow crystal growth to proceed under equilibrium control.[12] Such a condition is favored by the comparatively weak binding of M_b ions by alkoxide donor atoms as in $[\mathbf{2}]^-$.[11]

The purpose of this contribution is to present full details of the design and properties of a candidate magnetic linking unit, the di-Co^{III} complex of $[\mathbf{3}]^{8-}$, that is $[\mathbf{4}]^{2-}$, which has two $S = 1$ Co^{III} ions coordinated in a planar environment; $[PPh_4]_2[\mathbf{4}]$ is the first reported example of a coordination complex containing more than one planar cobalt(III) center. Upon one-electron oxidation of $[\mathbf{4}]^{2-}$ to $[\mathbf{4^I}]^-$, a significant magnetic exchange pathway is found for the two Co^{III} ions. It will be shown that $[\mathbf{4^I}]^-$ is a ferrimagnetic complex, in which a ligand radical is coupled antiferromagnetically with the two Co^{III} ions, thereby aligning the two Co^{III} spin systems in a common direction. Exchange-coupled metal–radical spin systems provide a powerful method for generating interesting magnetic materials.[13, 14] This approach has been somewhat limited in the past due to the comparative rarity of stable radical systems. We characterize herein the first example of a new class of stable metal–radical spin systems through a comparison of the chemical, physical, and magnetic properties of $[\mathbf{4}]^{2-}$ and $[\mathbf{4^I}]^-$ with their d^0–d^0 bis(V^V) analogues, $[\mathbf{5}]^{2-}$ and $[\mathbf{5^I}]^-$.

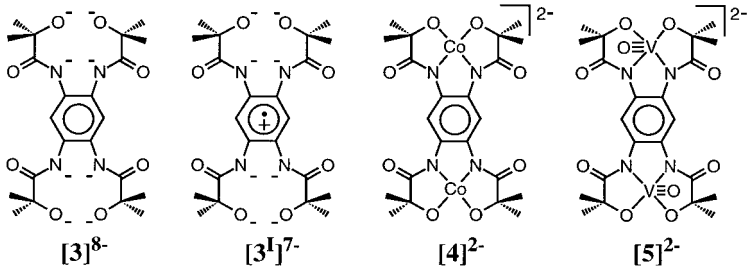

Results and Discussion

Ligand synthesis: The binucleating ligand, 1,2,4,5-tetrakis(2-hydroxy-2-methylpropanamido)benzene, $H_8[\mathbf{3}]$, was synthesized in a straightforward manner (Scheme 2). Overall yields of $H_8[\mathbf{3}]$ were good, >60% based on the starting tetraaminobenzene, and a favorable feature of the synthesis was that the intermediate 1,2,4,5-tetrakis(2-acetyloxy-2-methylpropanamido)benzene formed in high yield and did not need to be extensively purified for the hydrolysis step leading to $H_8[\mathbf{3}]$. The ligand $[\mathbf{3}]^{8-}$ binds two Co^{II} or $V^{IV}(O)$ centers to give, following air oxidation, the dimeric complexes, $[\mathbf{4}]^{2-}$ and $[\mathbf{5}]^{2-}$, respectively. $[\mathbf{3}]^{8-}$ is an idealized representation of the ligand without any metal centers. It is unlikely that such a highly charged species would be stable or soluble during the metallation process. We suspect that the insertion of the metal ions into a partially deprotonated ligand acts to enhance the deprotonation of the ligand framework, as the metal is chelated by the ligand, and $[\mathbf{4}]^{2-}$ or $[\mathbf{5}]^{2-}$ is produced.

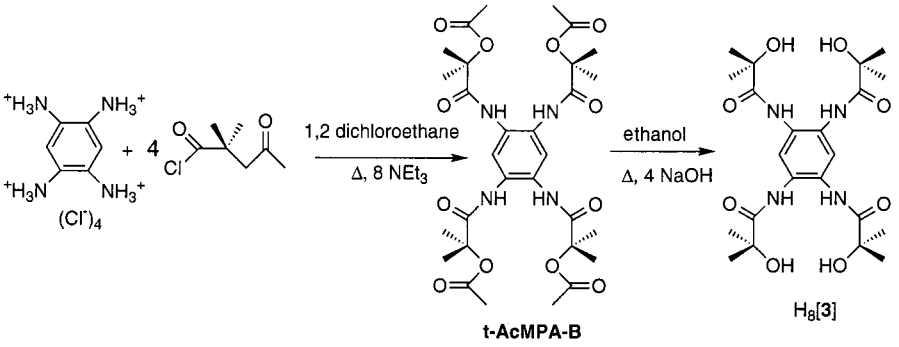

Scheme 2.

X-ray crystal structure of $[PPh_4]_2[\mathbf{4}]\cdot 2H_2O$: The result of the X-ray structural determination of $[\mathbf{4}]^{2-}$ is shown in Figure 1. Crystallographic data are given in Table 1, while selected bond lengths and angles are presented in Table 2. A single Co^{III} center comprises the repeating unit of the crystal, as the dianion is located at a crystallographic center of symmetry. The four donor atoms of the chelate ring lie almost exactly in a plane (largest deviation 0.010 Å) and the Co^{III} center sits essentially in the plane of the four donor atoms (deviation from the least squares plane 0.013 Å). Thus, the two metal centers are in planar four-coordinate environ-

0947-6539/98/0411-2174 $ 17.50+.50/0 *Chem. Eur. J.* **1998**, *4*, No. 11

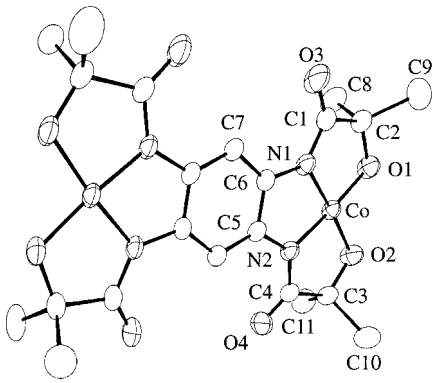

Figure 1. ORTEP diagram of the dianion in $[PPh_4]_2[\mathbf{4}]\cdot 2H_2O$; thermal probability ellipsoids are drawn to encompass 50% of the total electron density.

Table 1. Crystal and data-collection parameters for $[\mathbf{4}]^{2-}$ and $[\mathbf{5}]^{2-}$

	$[PPh_4]_2[\mathbf{4}]\cdot 2H_2O$	$[Et_4N]_2[\mathbf{5}]$
formula	$C_{35}H_{35}CoN_2O_5P$	$C_{19}H_{33}N_3O_5V$
M_r	653.59	434.43
crystal system	triclinic	monoclinic
space group	$P\bar{1}$	$P2_1/c$
a [Å]	10.937(2)	9.530(3)
b [Å]	11.274(3)	21.880(3)
c [Å]	13.192(2)	11.334(2)
α [°]	104.85(1)	90
β [°]	97.82(1)	113.77(2)
γ [°]	87.74(2)	90
V [Å^3]	1557.8(5)	2162.8(8)
Z	1	4
ρ_{calcd} [g cm^{-3}]	1.393	1.33
μ ($Mo_{k\alpha}$) [mm^{-1}]	6.71	5.20
crystal size [mm]	$0.40\times 0.35\times 0.20$	$0.26\times 0.21\times 0.14$
T [°C]	20(2)	18(1)
$2\theta_{max}$ [°]	50	51
h, k, l range	−14/14, −14/14, 0/17	−10/11, −26/0, −13/0
reflns collected	7886	4606
unique reflns	6699	4237
observed ($I>2\sigma I$)	5265	2839
abs correction	0.93–0.98	0.96–0.99
transmission		
parameters refined	404	385
$R_1=\Sigma \lvert\lvert F_o\rvert-\lvert F_c\rvert\rvert/\Sigma\lvert F_o\rvert$ (observed reflns)	0.040	0.041
wR_2	0.104	0.113

Table 2. Selected bond lengths [Å] and angles [°] for $[PPh_4]_2[\mathbf{4}]\cdot 2H_2O$

Co–O1	1.795(2)	C3–C4	1.532(4)
Co–O2	1.798(2)	C3–C10	1.526(5)
Co–N1	1.817(2)	C3–C11	1.516(5)
Co–N2	1.825(2)	C3–O2	1.423(4)
C1–C2	1.5329(4)	C4–N2	1.354(4)
C1–N1	1.354(4)	C4–O4	1.214(4)
C1–O3	1.225(4)	C5–C6	1.415(4)
C2–O1	1.423(4)	C5–N2	1.419(3)
C2–C8	1.537(5)	C6–C7	1.385(4)
C2–C9	1.519(5)	C6–N1	1.415(4)
O1–Co–O2	97.4(1)	N1–Co–O1	88.5(1)
N1–Co–N2	85.7(1)	N1–Co–O2	173.9(1)
N2–Co–O1	174.3(1)	N2–Co–O2	88.3(1)
		C3–C10	1.526(5)

ments. The Co–Co intramolecular nonbonded distance is 7.69 Å. The water molecules observed in the crystal are hydrogen bonded to amide oxygen atoms and there is no close contact of any water oxygen atom to the Co^{III} centers.

Crystals of $[PPh_4]_2[\mathbf{4}]\cdot 2H_2O$ have been characterized by other techniques to establish the purity of the bulk material. After vacuum drying at 80–100 °C for several hours, the dehydrated form is obtained as an analytically pure material. The dimer gives assignable, paramagnetically shifted ^{1}H NMR signals in CD_3CN (δ vs. TMS): CH_3 $\delta=9.9$, ArH $\delta=-0.8$.

X-ray crystal structure of $[Et_4N]_2[\mathbf{5}]$: The diamagnetic bis-$[V^V(O)]$ dimer, $[\mathbf{5}]^{2-}$, with d^0 metal ions was obtained for the purposes of comparing its chemical, physical, and magnetic properties with those of $[\mathbf{4}]^{2-}$. The results of an X-ray structural determination are depicted in Figure 2; crystallographic data are given in Table 1, while selected bond lengths

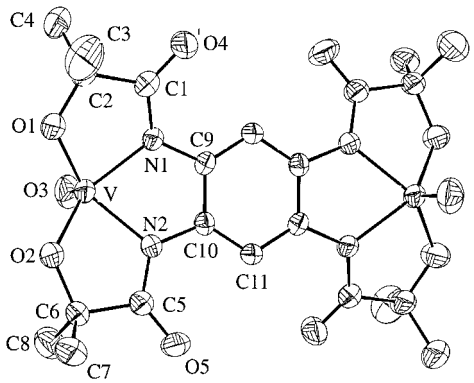

Figure 2. ORTEP diagram of the dianion in $[Et_4N]_2[\mathbf{5}]$; thermal probability ellipsoids are drawn to encompass 50% of the total electron density.

and angles are given in Table 3. The vanadyl groups are oriented in a *trans* fashion and there is a molecular inversion center. The V^V–O(3) bond length is 1.600 (3) Å, which is similar to those found for other square-pyramidal complexes, $[V(O)(acac)_2]$ (1.57 Å) (acac = acetylacetonate), $[V(O)(bzac)_2]$ (1.61 Å)[15] (bzac = benzoylacetone), and $[V^V(O)(\kappa^4$-

Table 3. Bond lengths [Å] and angles [°] for $[Et_4N]_2[\mathbf{5}]$

V–O3	1.600(3)	C5–O5	1.224(4)
V–O1	1.797(2)	C5–N2	1.344(4)
V–O2	1.809(2)	C6–C7	1.504(5)
V–N1	2.003(2)	C6–C8	1.515(5)
V–N2	2.010(2)	C6–O2	1.434(4)
C1–C2	1.536(4)	C9–C10	1.400(4)
C1–N1	1.352(4)	C9–C11	1.393(4)
C1–O4	1.226(4)	C9–N1	1.415(3)
C2–C3	1.513(6)	C10–C11#1[a]	1.391(4)
C2–C4	1.512(5)	N2–C10	1.411(3)
C2–O4	1.420(4)	C11-C10#1[a]	1.391(4)
C5–C6	1.536(4)	O3–V–O1	108.84(14)
O3–V–O2	108.20(13)	O3–V–N2	102.97(12)
O1–V–O2	106.27(11)	O1–V–N2	143.65(12)
O3–V–N1	105.06(12)	O2–V–N2	79.24(9)
O1–V–N1	79.43(10)	N1–V–N2	75.69(9)
O2–V–N1	141.93(10)		

[a] Symmetry transformations used to generate equivalent atoms: #1 = $-x+1, -y+1, -z+1$

HMPA-B)]$^-$ (1.598 (3) Å)[16] (HMPA-B = 2-hydroxy-2-methylpropanamido)benzene). The square plane in [**5**]$^{2-}$ defined by the ligand chelate atoms is distorted as the $V^V(O)$ moieties lie significantly closer to the alkoxide oxygen atoms, V–O1 1.791(2) Å and V–O2 1.809(2) Å, than to the amide nitrogen atoms, V–N1 2.003(2) Å and V–N2 2.010(2) Å. It is noteworthy that the amide nitrogen atoms are approximately 0.2 Å farther from the V center in [**5**]$^{2-}$ than from the Co center in [**4**]$^{2-}$ ($V-N_{av} = 2.006$ Å and $Co-N_{av} = 1.821$ Å); the V–O distances are similar to those in [**4**]$^{2-}$ ($V-O_{av} = 1.80$ Å and $Co-O_{av} = 1.796$ Å). The comparative displacement toward oxygen reflects the higher oxophilicity of vanadium compared with cobalt, which results from V–O π interactions. Another difference between [**5**]$^{2-}$ and [**4**]$^{2-}$ is that the vanadium is displaced 0.540 Å from the best fit plane through O1, O2, N1, N2, while Co^{III} lies essentially in the plane of the chelating atoms, 0.013 Å out of the best fit plane. The overall coordination environment around the vanadyl group is similar to the one found in $[V^V(O)(\kappa^4\text{-HMPA-B})]^-$.[16]

Electrochemistry: The cyclic voltammograms of [**4**]$^{2-}$ and [**5**]$^{2-}$ are remarkably similar. Both complexes show two well-separated, reversible one-electron oxidations ($E^{o'}_{ox,1}$ and $E^{o'}_{ox,2}$) and two closely spaced, reversible or quasireversible one-electron reductions ($E^{o'}_{red,1}$ and $E^{o'}_{red,2}$) (Figure 3, Table 4). The

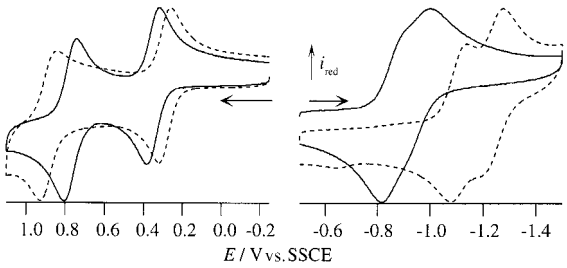

Figure 3. Cyclic voltammograms of $[PPh_4]_2$[**4**] (0.6 mM; —) and $[Et_4N]_2$[**5**] (0.98 mM; - - -) in 0.1M $TBAPF_6/CH_3CN$ ($\nu = 50$ mV s^{-1}).

Table 4. Electrochemical properties of $[PPh_4]_2$[**4**] and $[Et_4N]_2$[**5**][a]

	$E^{o'}_{ox,1}$[mV] (ΔE_p [mV])	$E^{o'}_{ox,2}$ [mV] (ΔE_p [mV])	$E^{o'}_{red,1}$ [mV] (ΔE_p [mV])	$E^{o'}_{red,2}$ [mV] (ΔE_p [mV])
[**4**]$^{2-}$	290 (60)	885 (82)	−1110 (60)	−1240 (76)
[**5**]$^{2-}$	350 (66)	770 (64)	−860 (84)	−965 (74)
1,4-$(NMe_2)_2$-C_6H_4	115 (70)	710 (80)	–	–

[a] Potentials are vs. SSCE in 0.1M $TBAPF_6/CH_3CN$

oxidized species are designated as [**4^I**]$^-$ and [**4^{II}**] for the cobalt dimer and [**5^I**]$^-$ and [**5^{II}**] for the vanadium dimer. The [**4^I**]$^-$/[**4^{II}**] couple becomes totally irreversible if the CH_3CN is wet. In the ligand environment found in both [**5**]$^{2-}$ and the analogous monomeric complex $[V^V(O)(\kappa^4 - \text{HMPA-B})]^-$,[14, 15] the vanadium centers are d^0; these diamagnetic species have been characterized by elemental analysis, X-ray structural determination, and ^{1}H NMR spectroscopy. The d^0 configuration of the vanadium centers in [**5**]$^{2-}$ allows one to conclude that the [**5**]$^{2-}$/[**5^I**]$^-$ and [**5^I**]$^-$/[**5^{II}**] oxidation processes are both ligand-centered. Thus, given the similar potentials for the oxidation events of both [**4**]$^{2-}$ and [**5**]$^{2-}$, we infer that the oxidations in [**4**]$^{2-}$ are also ligand-centered. EPR and UV-Vis data on [**4^I**]$^-$ and [**5^I**]$^-$, detailed below, demonstrate that the oxidation is localized on the aryl ring, that is [**4^I**]$^-$ and [**5^I**]$^-$ both contain **3^I**. It is noteworthy that $[PPh_4][Co^{III}(\kappa^4\text{-MAC*})]$[18] (MAC* = a tetraamido macrocycle, which has no aromatic ring, exhibits an irreversible oxidation at 1.14 V vs. SSCE (0.1M tBu_4NPF_6/CH_3CN), which we assign to the Co^{III}/Co^{IV} transformation. H_8[**3**] is insufficiently soluble to obtain its electrochemical properties. For 1,4-$(NMe_2)_2$-C_6H_4, an organic system related to [**4**]$^{2-}$ and [**5**]$^{2-}$, two reversible oxidations are observed in CH_3CN, the first oxidation forming the well known Wurster's blue cation radical (Table 4). In contrast, 1,2,4,5-$(NMe_2)_4$-C_6H_2 exhibits a single two-electron transfer forming a stable diamagnetic dication,[19] but a distortion of the ring accompanies the oxidation.

The one-electron oxidized dimers have different chemical stabilities. It is relatively straightforward to isolate [**4^I**]$^-$ as a solid material (see Experimental Section for details), but [**5^I**]$^-$ decomposes in the presence of light and/or light and air. Both [**4^{II}**] and [**5^{II}**] also readily decompose. As noted above, [**4^{II}**] is sensitive to water in the CH_3CN and is stable only on the seconds timescale. [**5^{II}**] is sensitive to light and/or light and air. Samples of [**5^{II}**] prepared by bulk electrolysis in the inert atmosphere glove box (< 5 ppm O_2) invariably contained [**5^I**]$^-$, and possibly [**5**]$^{2-}$, as determined by UV/Vis spectroscopy. A solution of [**5^{II}**], allowed to stand in the glove box, partially reconverts to [**5**]$^{2-}$.

The reductions of both dimers, [**4**]$^{2-}$ and [**5**]$^{2-}$, are most likely to be metal-centered events (Table 4). The measured reduction potentials reflect the facile air oxidation of the reduced forms observed synthetically. In monomeric diamido-*N*-dialkoxidocobalt complexes, Co^{III}/Co^{II} reductions occur between −0.8 and −1.0 V (vs. SSCE).[20] The Co^{III}/Co^{II} reductions are more negative in [**4**]$^{2-}$ because of its dianionic nature. In the case of [**5**]$^{2-}$, one assumes that the reduction events (Table 4) represent $V(O)^{V/IV}$ couples since it is improbable that the aromatic ring would be reducible at such mild potentials. The close spacing of the reductions (≈100 mV) implies that there is little electronic communication between the metals.

UV/Vis spectroscopy: Support for assignment of the one-electron oxidized product of the dimers to oxidation of the bridging π system comes from UV/Vis experiments. The [**4**]$^{2-}$ dianion was oxidized with $[Cp_2Fe]^+$, while [**5**]$^{2-}$ was best oxidized by bulk electrolysis; both oxidations were performed in CH_3CN. However, because [**5^I**]$^-$ is light/air sensitive, it was not possible to quantitate accurately the number of electrons passed during the oxidation or to assign molar extinction coefficients to the absorption bands. The result of a titration experiment for the oxidation of $[PPh_4]_2$[**4**] with $[Cp_2Fe]PF_6$ is shown in Figure 4. Three isosbestic points occur at $\lambda = 706$, 486, and 428 nm and new absorption bands appear in the visible region at $\lambda_{max} = 652$, 548, and $\lambda = 508$ nm (sh). These new absorption bands are similar to those found for Wurster's blue, $\lambda_{max} = 606$ and 560 nm. In other amine-substituted aromatic radical cations, band shapes, absorption energies, and absorption intensities are sensitive to the substitution pattern on

0947-6539/98/0411-2176 $ 17.50+.50/0 *Chem. Eur. J.* **1998**, *4*, No. 11

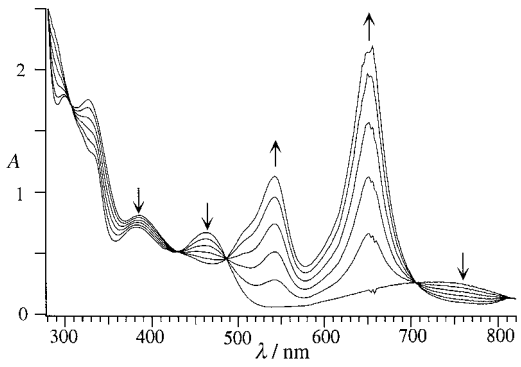

Figure 4. UV/Vis spectra taken of the oxidation of $[PPh_4]_2$[**4**] with $[Cp_2Fe]PF_6$ in CH_3CN to form $[PPh_4]$[$\mathbf{4^I}$]. Each trace after the starting spectrum (0 equiv) corresponds to the addition of 0.2 equivalents of oxidant.

the aromatic ring.[21] Likewise, [$\mathbf{5^I}$]$^-$ exhibits new absorptions in the visible region at $\lambda = 604$ (sh), and $\lambda_{max} = 598$, and 552 nm (Figure 5). Compound [$\mathbf{5^{II}}$] was also prepared by bulk

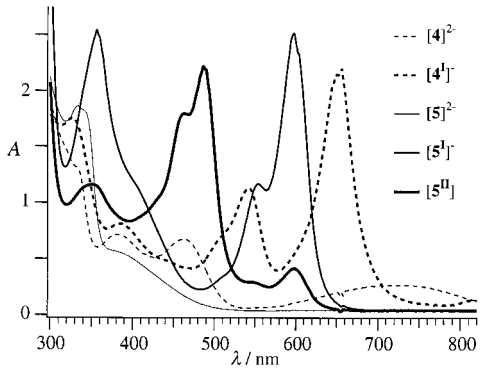

Figure 5. UV/Vis traces of $[PPh_4]_2$[**4**], $[PPh_4]$[$\mathbf{4^I}$], $[Et_4N]_2$[**5**], $[Et_4N]$[$\mathbf{5^I}$], and [$\mathbf{5^{II}}$] in CH_3CN $[PPh_4]$[$\mathbf{4^I}$] was prepared by oxidation with $[Cp_2Fe]^+$, while $[Et_4N]$[$\mathbf{5^I}$], and [$\mathbf{5^{II}}$] were prepared by bulk electrochemical oxidation. Legend is shown in figure.

electrolysis and the UV/Vis spectrum of a freshly prepared sample is shown in Figure 5. The spectrum of [$\mathbf{5^{II}}$] is similar to that for [$\mathbf{5^I}$]$^-$, but the absorption bands are shifted to higher energy, $\lambda_{max} = 486$ and 462 nm (the weak absorption at 598 nm probably arises from unoxidized [$\mathbf{5^I}$]$^-$ or decomposed [$\mathbf{5^{II}}$]).

EPR spectroscopy of $[PPh_4]$[$\mathbf{4^I}$] and $[Et_4N]$[$\mathbf{5^I}$]: The EPR spectrum in CH_2Cl_2 at 44 K of $[PPh_4]$[$\mathbf{4^I}$], prepared by bulk electrochemical oxidation, is shown in Figure 6. This rhombic spectrum, with molecular g values of $g_z = 1.98$, $g_x = 4.01$, and $g_y = 5.63$, indicates that the ground state has a total spin, S_T, of 3/2. The EPR spectrum at 44 K of $[Et_4N]$[$\mathbf{5^I}$], also prepared by bulk electrochemical oxidation (Figure 7), shows only a $g = 2$ resonance indicative of an isotropic organic radical species, linewidth ≈ 22 G. We investigated the EPR spectrum of $[Et_4N]$[$\mathbf{5^I}$] at room temperature in solution in order to detect the presence of nitrogen or vanadium hyperfine interactions. A singlet with a linewidth of ≈ 6 G was observed at ambient temperature. As [$\mathbf{5^I}$]$^-$ has two vanadium ($I = 7/2$) and four nitrogen atoms ($I = 1$), the narrow linewidth at ambient

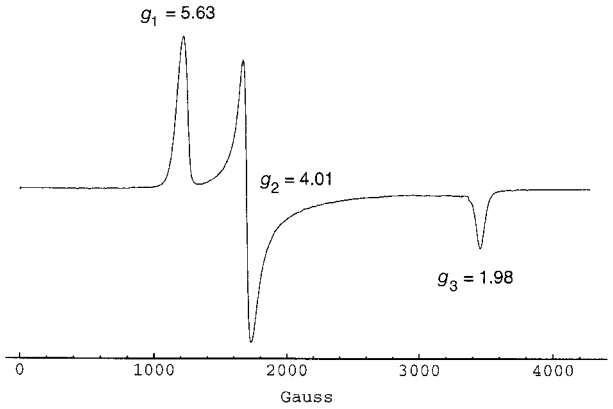

Figure 6. Low-temperature (44 K) EPR spectrum in frozen CH_2Cl_2 solution of $[PPh_4]$[$\mathbf{4^I}$] prepared by bulk electrochemical oxidation in the absence of air.

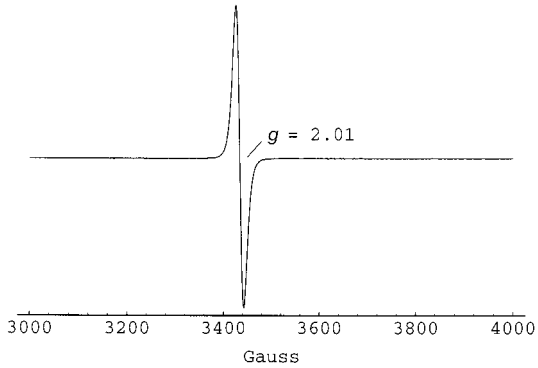

Figure 7. Low-temperature (44 K) EPR spectrum in frozen CH_3CN solution of $[Et_4N]$[$\mathbf{5^I}$] prepared by bulk electrochemical oxidation in the absence of air.

temperature indicates the magnitude of vanadium or nitrogen hyperfine coupling to be small. For comparison purposes, the V^{IV} monomeric analogue of [**5**]$^{2-}$, $[V^{IV}O(\kappa^4\text{-HMPA-B})]^{2-}$, exhibits vanadium hyperfine coupling constants of $A_\perp = 46$, $A_\parallel = 157$ G,[22] while the Wurster's blue cation radical exhibits hyperfine coupling to the aromatic hydrogen atoms of 20 G and to the N atoms of 70 G.[23] Thus, the EPR data for $[Et_4N]$[$\mathbf{5^I}$] are consistent with the locus of oxidation being confined primarily to the π system of the aromatic ring portion of the molecule.

Magnetic susceptibility studies of $[PPh_4]_2$[4**] and $[PPh_4]$[$\mathbf{4^I}$]**: The SQUID magnetic susceptibility data (μ_{eff} vs. T plots) for $[PPh_4]_2$[**4**] in dehydrated form are shown in Figure 8. The best fit parameters to the data of Figure 8 under the constraints of three different models are summarized in Table 5. Model 1 is based on an approach employed[22, 23] for anisotropic planar Co^{III} centers, while models 2 and 3 utilize the calculational protocol given in the Experimental Section. For models 1 and 2, where $J_{Co^{III}\text{-}Co^{III}} = 0$, axial g tensors and large D values were found (Table 5). These g and D values agree well with those determined for planar Co^{III}-containing monomeric analogues of [**4**]$^{2-}$, $[Co^{III}(\kappa^4\text{-HMPA-B})]^-$, $g_\perp = 2.2$, $g_\parallel = 2.5$, and $D = 45$ cm^{-1}[26] and $[Co^{III}(\kappa^4\text{-PAC*})]^-$ (PAC* = bis-hydroxy methyl propanamidodimethylpentanone), $g_\perp = 2.03$ and $g_\parallel = 2.65$, and $D = 373$ cm^{-1}.[11] If $J_{Co^{III}\text{-}Co^{III}}$ was employed as a fitting

Table 5. Atomic and molecular parameters for $[\mathbf{4}]^{2-}$ and $[\mathbf{4^I}]^{-}$ derived from magnetic susceptibility and EPR spectroscopy data under the constraints of several different exchange coupling models

	Model	Comment	$g_{Co^{III}}$			$ZFS_{Co^{III}}$		J_{ij} [cm^{-1}]		R	$g_{molecular}$		
			g_{1x}	g_{1y}	g_{1z}	D[cm^{-1}]	E/D	Co^{III}–Co^{III}	$Co^{III}-\mathbf{3^I}$	$\times 10^5$	g_x	g_y	g_z
$[\mathbf{4}]^{2-}$	1[a]	axial	2.03	2.03	2.43	79.2				0.22			
$[\mathbf{4}]^{2-}$	2	≈ axial	2.0[b]	2.04	2.44	78.5	0.01	0[b]		0.25			
$[\mathbf{4}]^{2-}$	3	≈ isotropic	2.16	2.16	2.17	81.0	0[b]	4.0		0.30			
$[\mathbf{4^I}]^{-}$	4[c]	rhombic	2.86	2.68	2.19[d]	76.2	0.19		75.9	2.8	4.04[e]	5.76[e]	2.05[e]
$[\mathbf{4^I}]^{-}$		EPR data									4.01	5.63	1.98

[a] A model similar to that employed for anisotropic monomeric cobalt species[24] was employed. [b] Fixed during fitting. [c] For calculational purposes, the g value for the organic radical $\mathbf{3^I}$ or $(\kappa^4-\mathbf{3}\text{-}\kappa^4)^{I}$ was considered to be isotropic and fixed at 20 as observed in the EPR spectrum of $[\mathbf{5^I}]^{-}$. [d] In order to return the correct molecular spectroscopic g_z value near 2.0, g_{1z} for the Co^{III} centers was allowed to vary only between 2 and 2.2. [e] Molecular g values were calculated from the best fit parameters derived from the magnetic susceptibility data.

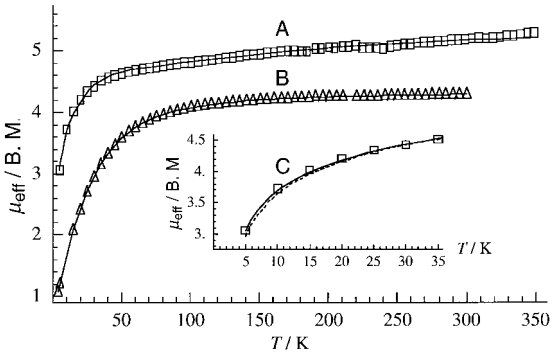

Figure 8. Magnetic susceptibility data for $[PPh_4]_2[\mathbf{4}]$ (△) at 0.5 T, and $[PPh_4][\mathbf{4^I}]$ (□) at 5 T. The lines are theoretical fits to the data as described in the text. The inset shows the distinction between full powder averaging and $M_{av=}M_x/3+M_y/3+M_z/3$ for the rhombic $[PPh_4][\mathbf{4^I}]$ system.

parameter, model 3, a pseudoisotropic g tensor, a large D value, and a small $J_{Co^{III}-Co^{III}}$ were found (Table 5). The results of model 3 were rejected, because there was no improvement in the fit to the data and the fit leads to an isotropic g value, which does not accurately reflect the results obtained for monomeric Co^{III} analogues.

The value of $J_{Co^{III}-Co^{III}}$ is found to be essentially zero in $[PPh_4]_2[\mathbf{4}]$. This confirms that the large Co – Co separation of 7.7 Å precludes exchange by direct overlap. Furthermore, the aromatic bridging ligand in closed-shell form apparently does not provide an effective conduit for Co^{III} – Co^{III} magnetic communication. For related dimeric d^1 $V^{IV}O$ and d^9 Cu^{II} complexes in a Jager type[27–31] donor environment, exchange coupling values across a similar closed-shell aromatic bridge (based on a tetraaminobenzene core) were found to be $J_{V^{IV}O-V^{IV}O} \approx 0$ cm^{-1} and $J_{Cu^{II}-Cu^{II}} \approx 24$ cm^{-1} (antiferromagnetic).[30, 31] The exchange coupling values found for the Cu^{II} and V^{IV} Jager-type complexes were interpreted[32] in terms of a σ-based superexchange coupling pathway that depended on a single key magnetic orbital. This key orbital points directly at the ligand donor atoms and is half-filled for the Jager-type copper case and empty in both the Jager-type vanadium case and in $[PPh_4]_2[\mathbf{4}]$ (see Scheme 1).

The g values derived from powder magnetic susceptibility data tend to reflect an average g contribution, but are relatively insensitive to g value anisotropy as shown for $[PPh_4]_2[\mathbf{4}]$ in Table 5. A variety of different anisotropic g value combinations can be employed to fit the data, but the average g value of such combinations remains essentially constant at $g_{av} = 2.16$. Therefore, molecular g values measured from EPR spectroscopy can provide a valuable additional constraint on the atomic g values used to model magnetic data, particularly when g value anisotropy is present as in $[PPh_4][\mathbf{4^I}]$.

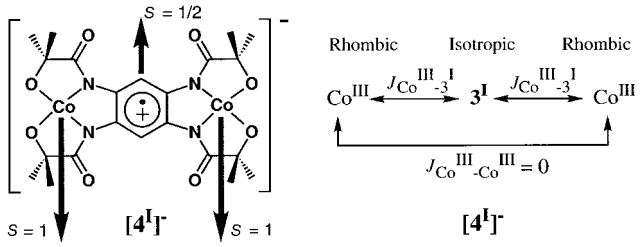

A plot of μ_{eff} versus T for $[PPh_4][\mathbf{4^I}]$ is shown in Figure 8. Qualitatively, the decrease in μ_{eff} with decreasing temperature is indicative of antiferromagnetic exchange coupling. In order to fit the magnetic susceptibility data for $[PPh_4][\mathbf{4^I}]$ and reproduce the rhombic $S_T = 3/2$ ground state observed by EPR spectroscopy, model 4 was employed. In model 4, two rhombic $S = 1$ Co^{III} centers are antiferromagnetically coupled to an intervening isotropic $S = 1/2$ species (that is $\mathbf{3^I}$) to yield a rhombic $S_T = 3/2$ ground state. This is the only model considered to be consistent with the combined EPR, electrochemical, and UV/Vis data for the dimeric d^6 Co^{III} and d^0 $V^{V}O$ complexes. For each least squares fit to the magnetic data, the molecular g values were calculated and compared to the values determined by EPR spectroscopy. The key result from model 4 is that J is large and of the same magnitude as D, $J \approx D \approx 76$ cm^{-1}. The agreement of D values for both $[PPh_4]_2[\mathbf{4}]$ and $[PPh_4][\mathbf{4^I}]$, $D \approx 76$ cm^{-1} and $D \approx 79$ cm^{-1}, respectively, suggests that the cobalt centers in both complexes reside in a similar ligand field potential. Therefore it is likely that the radical species resides in a portion of the molecule comparatively distant from the cobalt centers, that is on the aromatic ring and possibly the amide substituents as in $\mathbf{3^I}$. In comparison to the metal/π cation radical system reported here, we recently described[34] a monomeric Fe^{III}/ligand cation radical species[34], in which the exchange coupling between the $S = 3/2$ intermediate spin Fe^{III} and the π cation radical was also antiferromagnetic with $J \approx 300$ cm^{-1}.

0947-6539/98/0411-2178 $ 17.50+.50/0 *Chem. Eur. J.* **1998**, *4*, No. 11

Conclusion

The binucleating ligand $[\mathbf{3}]^{8-}$ provides a means for obtaining substantial magnetic communication between coordinated metal centers, when oxidized to the π cation radical $[\mathbf{3}^{\mathbf{I}}]^{7-}$. It is by design[35] that the ligand $[\mathbf{3}]^{8-}$ is made solely from oxidatively robust components, thereby allowing the formation of the stable ligand cation radical containing species, $[PPh_4]_2[\mathbf{4}^{\mathbf{I}}]$. The ligand donor groups also serve to shift the oxidation potentials of the metals to values beyond those of the aromatic ring. We have shown[11] that the strongly σ-donating ligand found in $[\mathbf{1}]^-$, which is related to $[\mathbf{3}]^{8-}$, can direct magnetic interactions between primary and secondary coordinated metal ions. Thus, $[\mathbf{4}^{\mathbf{I}}]^-$ could prove to be a useful building block for forming larger magnetic clusters and/or bulk magnetic materials,[10] a hypothesis that is the subject of ongoing study.

Experimental Section

Materials: All solvents were reagent grade (Aldrich or Fisher) and were used as received except for anhydrous pyridine (Aldrich, Sureseal) and CH_3CN, which was dried over CaH_2 for electrochemical measurements. 1,2,4,5-tetraaminobenzene · 4 HCl (Fluka), 1-chlorocarbonyl-1-methylethyl acetate, PPh_4Cl, anhydrous $CoCl_2$, and $VO(SO_4) \cdot 3H_2O$ (Aldrich) were reagent grade and used as received, while $[Cp_2Fe][PF_6]$ was prepared by a method described in the literature.[36]

Spectroscopic methods: ^1H NMR spectra were measured at 300 MHz and $^{13}C\{^1H\}$ NMR spectra were measured at 75.5 MHz on an IBM NR/300 FT-NMR spectrometer. Chemical shifts are reported in δ vs. $(CH_3)_4Si$ using residual solvent resonances as internal standards. Infrared data were obtained on a Nicolet 5DXB FT-IR or Mattson Galaxy 5000 spectrometer. UV/Vis data were taken on a Hewlett-Packard 8452A spectrophotometer, controlled by a Zenith Z-425/SX computer. Conventional X-Band EPR spectra were recorded in derivative mode on a IBM ESP300 spectrometer, equipped with a helium flow cryostat.

Electrochemical methods: Electrochemical measurements were performed by using a Princeton Applied Research Model 273 Potentiostat/Galvanostat, controlled with a Compudyne 486/DX computer. Current voltage curves were recorded on a Graphtec Model WX1200 X-Y recorder. The supporting electrolyte was 0.1 M $[n\mathrm{Bu}_4N][PF_6]$ ($TBAPF_6$, Fluka puriss) for cyclic voltammetry and 0.2 M $TBAPF_6$ for bulk electrolysis, CH_3CN or CH_2Cl_2 were used as solvents. Cyclic voltammetry was performed under N_2 or Ar in a three compartment cell using a glassy carbon disk working electrode ($A \approx 0.78$ or 7.1 mm^2), a Pt wire counterelectrode, and a sodium chloride saturated calomel electrode (SSCE) as reference electrode, while bulk electrolyses were carried out in a carbon crucible using a Pt wire counter electrode, and a Pt wire as a pseudoreference electrode.

Synthesis of (1,2,4,5-tetrakis-(2-acetyl-2-methylpropanamido)benzene, (*t*AcMPA-B): 1,2,4,5-tetraaminobenzene · 4 HCl (15 g, 0.053 mol), 1,2-dichloroethane (300 mL), and a magnetic stir bar were placed in a flask, which was fitted with a reflux condenser and a pressure equalizing addition funnel. The system was purged with N_2 for 20 min, then 1-chlorocarbonyl-1-methylethyl acetate (45.75 mL, 0.317 mol) was cannulated into the addition funnel and then added slowly (20 min) to the stirred solution. After all of the 1-chlorocarbonyl-1-methylethyl acetate was added, Et_3N (100 mL, 0.69 mol) was cannulated into the addition funnel, and then added dropwise to the stirred solution (1 h). After the Et_3N addition was complete, the system was heated to reflux and stirred under N_2 for 5 days, during which time $Et_3N \cdot HCl$ precipitated. After cooling the solution to room temperature, the solvent was removed under reduced pressure leaving a yellow solid. The solid was dissolved in CH_2Cl_2 (800 mL), and the solution was washed with 1.2 M HCl (4 × 400 mL) and then 1 M Na_2CO_3 (3 × 400 mL). The CH_2Cl_2 was removed under reduced pressure leaving a tan solid. The solid was slurried in pentane, filtered, and air dried to yield 31 g of crude *t*AcMPA-B. This material is sufficiently pure to be used for the preparation of $H_8[\mathbf{3}]$, or it can be recrystallized from acetone as follows. Impure *t*AcMPA-B (6 g) was dissolved in hot acetone (110 mL), the hot solution was rapidly suction filtered, and then the filtrate was cooled to −20 °C for 1–2 hours, during which time a white crystalline solid precipitated. The precipitate was recovered by filtration, washed with diethyl ether, and air dried to yield pure *t*AcMPA-B (5.61 g, recrystallization yield 93.5 %). ^1H NMR (CD_3CN): $\delta = 8.45$ (s, 4H, NH), 7.77 (s, 2H, C_6H_2), 2.08 (s, 12H, $C(O)CH_3$), 1.61 (s, 24H, CCH_3); ^{13}C NMR (CD_3CN): $\delta = 173.4$ (amide CO), 171.2 (acetyl CO), 129.3 (Ar CNHR), 121.8 (Ar CH), 81.5 (alkyl quaternary C) 25.2 (alkyl CH_3), 22.1 (acetyl CH_3); IR (nujol): $\tilde{\nu} = 3275$ (s, str, br, amide NH) 1740 (s, str, acetyl CO), 1667 (s, str, amide), 1610 cm^{-1}(sh, w, aryl ring/amide); $C_{30}H_{42}N_4O_{12}$ (650.68): calcd: C 55.38, H 6.51, N 8.61; found: C 55.48, H 6.49, N 8.57.

Synthesis of 1,2,4,5-tetrakis-(2-hydroxy-2-methylpropanamido)benzene, (H_8[3]): The unpurified *t*AcMPA-B (31.0 g), CH_3OH (1000 mL), NaOH (10.34 g, 0.25 mol, ≈4.4 equiv assuming pure *t*AcMPA-B), and a magnetic stir bar were placed in a flask, which was fitted with a reflux condenser. The system was flushed with N_2 (10 min) and then the mixture was refluxed under static N_2 (24 h). After cooling to room temperature, the CH_3OH was removed under reduced pressure yielding a tan solid, a mixture of $H_8[\mathbf{3}]$, and sodium acetate. The solid was placed in a beaker containing a 2:1 CH_3OH/H_2O mixture and the slurry heated to boiling. The slurry was cooled to 10–15 °C and then filtered. Most of the $H_8[\mathbf{3}]$ was insoluble in the CH_3OH/H_2O mixture, but the sodium acetate was soluble. The slurry was filtered while still at ≈15 °C and the white solid product was air dried (yield 1.78 g, 70 % based on 1,2,4,5-tetraaminobenzene tetrahydrochloride). ^1H NMR (DMSO[D6]): $\delta = 9.5$ (s, 4H, NH), 7.7 (s, 2H, C_6H_2), 5.8 (s, 4H, COH), 1.2 (s, 24H, CCH_3); IR (nujol): $\tilde{\nu} = 3449$, 3305, 3219, (OH alcohol, NH amide), 1656, 1630 (amide) cm^{-1}; $C_{22}H_{34}N_4O_8$ (482.54): calcd: C 54.76, H 7.10, N 11.6; found: C 54.64, H 7.05, N 11.55.

Synthesis of bis-tetraphenylphosphonium-di-cobalt(III)-κ^4:κ^4-(1,2,4,5-tetrakis-(2-hydroxy-2-methylpropanamido)benzene), ($[PPh_4]_2$[4]): $H_8[\mathbf{3}]$ (2.01 g, 4.11 mmol), 400 mL CH_3OH, anhydrous $CoCl_2$ (1.3 g, 10.0 mmol), NaOH (1.18 g, 29.5 mmol), and a magnetic stir bar were placed in a flask in air and the resulting slurry was stirred at room temperature for 2 days to yield a homogeneous green-brown solution. $[PPh_4]Cl$ (4.61 g, 12.3 mmol, 3 equiv) was added with stirring (2 h). Larger quantities of $[PPh_4]Cl$ have been used, with a substantial increase in yield, but the product is more time-consuming to isolate. The CH_3OH was then removed under reduced pressure, leaving a dark green-brown solid, which was dissolved with stirring in CH_2Cl_2 (800 mL, 24 h). The solution was filtered and the CH_2Cl_2 removed in vacuo. The resulting dark green solid was triturated with a stir bar in dry diethyl ether, filtered, and then air dried to yield a mixture of $[PPh_4]_2[\mathbf{4}]$ and $[PPh_4]Cl$. The unpurified dark green powder was placed in flask containing CH_3CN (50 mL), the slurry was stirred, heated to boiling, and then cooled to −20 °C. The resulting dark green precipitate was suction filtered and air dried. This washing of the solid was performed one more time to yield a dark green solid (2.65 g, 2.08 mmol, yield 50.7 %). A second crop of material was obtained by combining the CH_3CN washes, reducing the solution volume to 30–40 mL, and then allowing diethyl ether vapor to diffuse into the CH_3CN solution. After ≈five–seven days, the dark green crystals were separated from the white $[PPh_4]Cl$ crystals and air dried (0.2 g). The combined yield of $[PPh_4]_2[\mathbf{4}]$ from $H_8[\mathbf{3}]$ was 54.5 %. The number of water molecules varies from zero to two depending upon recrystallization and storage conditions, as shown by elemental analysis and NMR data. The stoichiometry of the sample used for elemental analysis was supported by ^1H NMR data. The crystal used for crystallographic analysis had two water molecules in the lattice for each $[PPh_4]_2[\mathbf{4}]$. ^1H NMR (CD_3CN): $\delta = 9.8$ (s, 24H, alkyl CH_3), 7.4, 7.22, 7.18, 7.155 (40H, aryl of $[PPh_4]^+$), 3.2 (H_2O), −0.8 (s, 2H, ArH); IR (nujol): $\tilde{\nu} = 1632$ cm^{-1} (amide); UV/Vis (95 % ethanol): λ_{max} (ε) = 238 (68000), 376 (10000), 468 (7300), 766 nm (2600); $C_{70}H_{66}N_4O_8Co_2P_2$ (1271.14) · 1.5 H_2O (27): calcd: C 64.77, H 5.36, N 4.32, P 4.77; found: C 64.86, H 5.35, N 4.41, P 4.55.

Synthesis of tetraphenylphosphonium-di-cobalt(III)-κ^4:κ^4-(1,2,4,5-tetrakis-(2-hydroxy-2-methylpropanamido)benzene), ($[PPh_4][\mathbf{4}^{\mathbf{I}}]$): $[PPh_4]_2[\mathbf{4}]$ (243 mg, 0.19 mmol), CH_2Cl_2 (15 mL), and a magnetic stir bar were placed in a Schlenk flask in air. The solution was deoxygenated with N_2 and then freshly prepared,[36] solid $[Cp_2Fe][PF_6]$ (63 mg, 0.19 mmol) was added. The solution immediately turned deep purple. The mixture was stirred under N_2 (1 h) and then exposed to air (30 min). A small amount of white solid

precipitate was removed by filtration in air and then the CH_2Cl_2 was removed in vacuo. The remaining purple-black solid product was washed copiously with toluene (500–700 mL) to remove ferrocene and then diethyl ether (≈200 mL). The purple powder was dissolved in a minimum amount of 1,2-dichloroethane, and pentane vapor was diffused into the 1,2-dichloroethane solution. After a few days, the purple-black crystalline product was collected by suction filtration, washed with pentane, and air dried (148 mg, 75 % yield). The solid was stored in a glove box under Ar. IR (KBr): $\tilde{\nu} = 1687\ cm^{-1}$ (s, amide); UV/Vis (1,2-dichloroethane): λ_{max} (ε) = 274 (37400), 300 (21050), 326 (20700), 387 (10000), 508 (8300), 548 (15000), 652 (29850), 816 (2000); $C_{46}H_{46}N_4O_8Co_2P$ (931.74) · $C_2H_4Cl_2$ (98.96): calcd: C 55.94, H 4.89, N 5.44; found: C 55.68, H 4.89, N 5.42. Presence of 1,2-dichloroethane in the solid was confirmed by a 9.6 % weight loss by TGA measurement.

Synthesis of bis-tetraethylammonium-di-vanadyl(v)-κ^4:κ^4-(1,2,4,5-tetrakis-(2-hydroxy-2-methylpropanamido)benzene), ([Et$_4$N]$_2$[5]): H_8[**3**] (1.52 g, 3.15 mmol) and $V^{IV}(O)(SO_4) \cdot 3H_2O$ (1.52 g, 7 mmol) were combined and dissolved in air in MeOH (175 mL). [Et_4N][OH] (20 wt % in H_2O, 16.6 mL, 22.1 mmol) was added and the mixture stirred overnight under air. A clear dark green solution formed. Removal of the solvent at reduced pressure yielded an oil, to which was added absolute EtOH (300 mL), which was then removed at reduced pressure leaving a green waxy solid. The wax was triturated with a stir bar in dry Et_2O (350 mL, 24 h) and then filtered. The crude product was dissolved in CH_3CN (100 mL), filtered, and then Et_2O vapor was diffused into the CH_3CN solution, depositing a mixture of [Et_4N]$_2$[**5**] and [Et_4N]$_2$[SO_4]. These solids were separated by spreading them on a double layer of filter paper, placing a second double layer of filter paper, and a glass plate on top of the solids, and allowing the hygroscopic [Et_4N]$_2$[SO_4] salt to be drawn into the filter paper (overnight in moist air). After the [Et_4N]$_2$[**5**] was scraped off the paper, it was recrystallized from a 1:1 CH_3CN:EtOH mixture by vapor diffusion of Et_2O. ^1H NMR (CD_3CN): $\delta = 8.35$ (s, 2H, ArH), 3.05 (q, 16H, NCH_2CH_3), 1.66 (s, 12H, CCH_3), 1.38 (s, 12H, CCH_3), 1.14 (tr, 24H, NCH_2CH_3); IR (KBr): $\tilde{\nu} = 1630$ (C=O amide), 965 (V≡O) cm^{-1}; $C_{38}H_{66}N_6O_{10}V_2$ (868.87): calcd: C 52.53, H 7.66, N 9.67; found: C 52.32, H 8.02, N 9.40.

Crystal structure determinations: Single crystals of [PPh_4]$_2$[**4**] · $2H_2O$ were grown by allowing Et_2O vapor to diffuse into a concentrated CH_3CN solution of [PPh_4]$_2$[**4**]. Green crystals of [PPh_4]$_2$[**4**] · $2H_2O$ were mounted on glass fibers on a Nonius CAD-4 diffractometer. Unit cell dimensions were determined from the four-circle coordinates of 25 reflections, well distributed through space. Data were collected with $\omega/2\theta$ scans using Zr-filtered $Mo_{K\alpha}$ radiation at room temperature with intensity control and orientation standards showing no significant variation during data collection. The data were corrected for Lorentz and polarization effects, and absorption applied using empirical phi scans.[37] The structure was solved by conventional Patterson and Fourier techniques[38] and refined by full-matrix least squares.[39] In the final cycles, all non-hydrogen atoms for [PPh_4]$_2$[**4**] · $2H_2O$ were allowed to assume anisotropic motion. Hydrogen atoms were located and held in idealized geometry with a single common thermal parameter. The refinements converged to residuals of 0.039 for [PPh_4]$_2$[**4**] · $2H_2O$. Crystal data and structure refinement parameters for [PPh_4]$_2$[**4**] · $2H_2O$ are found in Table 1.

Single crystals of [Et_4N]$_2$[**5**] were obtained by diffusing Et_2O vapor into a 1:1 CH_3CN/EtOH solution of [Et_4N]$_2$[**5**]. An intense green crystal of [Et_4N]$_2$[**5**] was mounted on a glass fiber on a Nonius CAD-4 diffractometer. A total of 4237 unique reflections ($2^\circ < 2\theta < 5^\circ$) were collected using $\omega/2\theta$ scans with graphite-monochromated $Mo_{K\alpha}$ X-radiation. Absorption corrections were by psi scans.[37] Structure solution was by direct methods employing SHELXS.[40] All hydrogen atoms were located in a difference map and were refined individually with isotropic temperature factors. Refinement by full-matrix least-squares on F^2 was carried out using SHELXL-92.[41] Atomic scattering factors and dispersion corrections were taken from the International Tables for Crystallography.[42] Refinement converged with $R_1 = 0.0399$ for 2839 observed reflections [$I > 2\sigma(I)$]. Crystal data and structure refinement parameters for [Et_4N]$_2$[**5**] are found in Table 1.

Further details of the crystal structure investigations for the structures reported in this paper, dianions [**4**]$^{2-}$ and [**5**]$^{2-}$ can be obtained from the Fachinformationszentrum Karlsruhe, D-76344 Eggenstein-Leopoldshafen (Germany), (fax: (+49) 7247-808-666; e-mail: crysdata@fiz.karlsruhe.de) on quoting the depository numbers CSD-408464 for [**4**]$^{2-}$, and CSD-408463 for [**5**]$^{2-}$.

Measurement and fitting of magnetic susceptibility data: Magnetic susceptibility measurements were performed on a Quantum Design SQUID magnetometer on dried powder samples of [PPh_4]$_2$[**4**] (5–300 K, 0.5 T) and [PPh_4][**4^I**] (5–350 K, 5 T). Diamagnetic corrections were applied to the data based on Pascal's constants or on values derived from measurements performed on mixtures of the free ligand and [PPh_4]Cl. All exchange coupling constants, J, are reported according to a $J\ S_i \cdot S_j$ convention, which yields ferromagnetic exchange couplings to be negative in sign.

Susceptibility data was fitted under the constraints of an eigenvalue matrix, derived from the spin only Hamiltonian shown in Equation (1).

$$H = 1/2\sum_{i,j} J_{ij}\hat{S}_i\hat{S}_j + \sum_i [D\left(\hat{S}_{zi}^2 - \frac{S_i(S_i+1)}{3}\right) + E(\hat{S}_{xi}^2 - \hat{S}_{yi}^2) + \hat{S}_i\hat{\mathbf{g}}_i\hat{H}] \quad (1)$$

The Hamiltonian matrix was diagonalized numerically for each field direction and the resulting eigenvalues utilized to calculate the magnetization along that direction using the thermodynamic relation given in Equation (2).

$$M = NkT\left(\frac{\partial lnZ}{\partial H}\right)_T \quad (2)$$

When necessary powder averaging was calculated over 49 unique orientations of the magnetic field, and weighted according to a normal vector approach. Minimization of R values as defined[9] by Equation (3) was accomplished by using the simplex method.[43] All calculations were performed by using the Mathematica language.[44]

$$R = \frac{\sum_{i=1}^{n} [\mu_{eff.exp}(T_i) - \mu_{eff.theo}(T_i)]^2}{\sum_{i=1}^{n} [\mu_{eff.exp}(T_i)]^2} \quad (3)$$

Acknowledgments: We gratefully acknowledge the NIH for support to T.J.C. (GM44867) and UC Boulder for support to G.T.Y. We also wish to thank Dr Maria Faldeaki at NIST in Boulder for magnetic measurements and Prof. Eckard Münck at CMU for helpful discussions.

Received: March 26, 1998 [F1068]

[1] H. Tamaki, Z. J. Zhuang, N. Matsumoto, S. Kida, M. Koikawa, N. Achiwa, Y. Hashimoto, H. Okawa, *J. Am. Chem. Soc.* **1992**, *114*, 6974–6979.
[2] H. Oshio, U. Nagashima, *Inorg. Chem.* **1992**, *31*, 3295–3301.
[3] O. Kahn, *NATO ASI Series C, Vol. 484*, Kluwer Academic, Dordrecht, **1996**, p. 660.
[4] D. Gatteschi, O. Kahn, J. S. Miller, F. Palacio, *NATO ASI Series E, Vol. 198* Kluwer Academic, Dordrecht, **1991**, p. 411.
[5] E. Coronado, C. J. Gomez-Garcia, J. J. Borras-Almenar, *J. Appl. Phys.* **1990**, *67(9)*, 6009–6010.
[6] S. Decurtins, H. W. Schmalle, P. Schneuwly, J. Ensling, P. Gutlich, *J. Am. Chem. Soc.* **1994**, *116*, 9521–9528.
[7] R. D. Willett, D. Gatteschi, O. Kahn, *NATO ASI Series C, Vol. 140*, D Reidel, Dordrecht, **1983**, p. 616.
[8] P. J. Hay, J. C. Thibeault, R. H. Hoffmann, *J. Am. Chem. Soc.* **1975**, *97*, 4884–4899.
[9] Y. Pei, Y. Journaux, O. Kahn, *Inorg. Chem.* **1989**, *28*, 100–103.
[10] T. J. Collins, S. W. Gordon-Wylie, E. L. Bominaar, C. P. Horwitz, G. Yee in *Magnetism: A Supramolecular Function*, *Vol. 484 NATO ASI Series C*, (Ed.: O. Kahn), Kluwer, **1996**, pp. 509–529.
[11] S. W. Gordon-Wylie, E. L. Bominaar, T. J. Collins, J. M. Workman, B. L. Claus, R. E. Patterson, S. E. Williams, B. J. Conklin, G. T. Yee, S. T. Weintraub, *Chem. Eur. J.* **1995**, *1*, 528–537.
[12] J. M. McBride, *Angew. Chem.* **1989**, *330*, 337; *Angew. Chem. Int. Ed. Engl.* **1989**, *28*, 377–379.
[13] A. Caneschi, D. Gatteschi, P. Rey, R. Sessoli, *Acc. Chem. Res.* **1989**, *22*, 392–398.
[14] N. Koga, Y. Ishimaru, H. Iwamura, *Angew. Chem.* **1996**, *108*, 802–804; *Angew. Chem. Int. Ed. Engl.* **1996**, *35*, 755–757.
[15] P. K. Hon, R. L. Belford, C. E. Pfinger, *J. Chem. Phys.* **1965**, *43*, 3111–3115.

[16] C. R. Cornman, K. M. Geiser-Bush, P. Singh, *Inorg. Chem.* **1994**, *33*, 4621 – 4622.
[17] C. R. Cornman, G. J. Colpas, J. D. Hoeschele, J. Kampf, V. L. Pecoraro, *J. Am. Chem. Soc.* **1992**, *114*, 9925 – 9933.
[18] T. J. Collins, E. S. Uffelman, *Angew. Chem.* **1989**, *101*, 1552; Angew. *Chem. Int. Ed. Engl.* **1989**, *28*, 1509 – 1511.
[19] K. Elbl, C. Krieger, H. A. Staab, *Angew. Chem.* **1986**, *98*, 1024; *Angew. Chem. Int. Ed. Engl.* **1986**, *25*, 1023 – 1024.
[20] T. J. Collins, T. G. Richmond, B. D. Santarsiero, B. G. R. T. Treco, *J. Am. Chem. Soc.* **1986**, *108*, 2088 – 2090.
[21] L. Michaelis, M. P. Schubert, S. Granick, *J. Am. Chem. Soc.* **1939**, *61*, 1981 – 1992.
[22] C. R. Cornman, E. P. Zovinka, Y. D. Boyajian, K. M. Geiser-Bush, P. D. Boyle, P. Singh, *Inorg. Chem.* **1995**, *34*, 4213 – 4219.
[23] V. Vatanen, J. A. Pedersen, *J. Chem. Soc. Perkin Trans 2* **1996**, 2207 – 2212.
[24] P. L. Birker, J. J. Bour, J. J. Steggerda, *Inorg. Chem.* **1973**, *12*, 1254 – 1259.
[25] P. J. van der Put, A. A. Schilperood, *Inorg. Chem.* **1974**, *13*, 2476 – 2479.
[26] D. M. Eichorn, J. Telser, C. L. Stern, B. M. Hoffman, *Inorg. Chem.* **1994**, *33*, 3533 – 3537.
[27] E.-G. Jäger, *Z. Chem.* **1968**, *8*, 30.
[28] E.-G. Jäger, *Z. Chem.* **1964**, *4*, 436 – 437.
[29] E.-G. Jäger, *Z. Chem.* **1968**, *8*, 392 – 393.
[30] E.-G. Jäger, *Z. Anorg. Allg. Chem.* **1969**, *364*, 177 – 191.
[31] L. Wolf, E-G. Jäger, *Z. Anorg. Allg. Chem.* **1966**, *346*, 76 – 91.
[32] E. F. Hasty, T. J. Colburn, D. N. Hendrickson, *Inorg. Chem.* **1973**, *12*, 2414 – 2421.
[33] D. N. Hendrickson in *Magneto-Structural Correlations in Exchange Coupled Systems*, (Eds.: R. D. Willet, D. Gatteschi, O. Kahn), D. Reidel, Dordrecht, **1985**, pp. 523 – 554.
[34] M. J. Bartos, C. Kidwell, K. E. Kauffmann, S. W. Gordon-Wylie, T. J. Collins, G. R. Clark, E. Münck, S. T. Weintraub, *Angew. Chem.* **1995**, *107*, 1345 – 1348; *Angew. Chem. Int. Ed. Engl.* **1995**, *34*, 1216 – 1219.
[35] T. J. Collins, *Acc. Chem. Res.* **1994**, *27*, 279 – 285.
[36] E. S. Yang, M. S. Chan, A. C. Wahl, *J. Phys. Chem.* **1975**, *79*, 2049 – 2051.
[37] A. C. North, D. C. Phillips, F. S. Mathews, *Acta Crystallogr. Sect. A* **1968**, *24*, 351 – 359.
[38] G. M. Sheldrick, *Program for Crystal Structure Solution, SHELX-76,* University Chemical Laboratory, **1976**.
[39] Scattering curves and dispersion corrections were taken from: *International Tables for X-ray crystallography, Vol. IV*, Kynoch Press, Birmingham, **1974**.
[40] G. M. Sheldrick, *Acta Crystallogr. Sect. A* **1990**, *46*, 467.
[41] G. M. Sheldrick, A program for Crystal Structure Solution, SHELX-92, University of Göttingen, **1992**.
[42] A. J. C. Wilson, *International Tables for Crystallography, Vol. C*, Kluwer, Dordrecht, **1992**.
[43] W. H. Press, B. P. Flannery, S. A. Teukolsky, W. T. Vetterling, *Numerical Recipes, The Art of Scientific Computing*, University Press, Cambridge, **1989**.
[44] S. Wolfram, *Mathematica, A System For Doing Mathematics By Computer*, Redwood City, CA, **1991**.

  0947-6539/98/0411-2181 $ 17.50+.25/0